Imaging the time-dependent structure of a molecule as it undergoes dynamics

F. Légaré,[1,2] Kevin F. Lee,[1,3] I. V. Litvinyuk,[1,4] P. W. Dooley,[1,3] A. D. Bandrauk,[2] D. M. Villeneuve,[1] and P. B. Corkum[1]
[1]*National Research Council of Canada, Ottawa, Ontario, Canada K1A 0R6*
[2]*Département de Chimie, Université de Sherbrooke, Sherbrooke, Québec, Canada J1K 2R1*
[3]*Department of Physics & Astronomy, McMaster University, Hamilton, Ontario, Canada K1S 5P3*
[4]*Department of Physics, Kansas State University, Manhattan, Kansas, 66506, USA*
(Received 6 October 2004; revised manuscript received 24 August 2005; published 23 November 2005)

We image the dynamics of diatomic and triatomic molecules with sub-5 fs and sub-Å resolution using laser Coulomb explosion imaging with 8 fs pulses. We obtain image information by measuring the vector momenta of all atomic ions produced by explosion of a single molecule. We image vibrating D_2^+ and of dissociating SO_2^{2+} and SO_2^{3+}. Images taken at 0 and 60 fs show that the dissociation of SO_2^{2+} produces an SO^+ rotational wave packet.

DOI: 10.1103/PhysRevA.72.052717 PACS number(s): 34.50.Gb, 33.80.Rv

Molecules have $3N$-3 coordinates (where N is the number of atoms) as well as time. Pump-probe spectroscopy [1] takes a low-dimensional projection of this inherently multidimensional problem. Hidden from view in most ultrafast dynamics experiments are unobserved changes to the molecular structure.

Measuring molecular structure requires that the wavelength of the probe is shorter than the length of the chemical bonds. Electron diffraction [2] can determine the structure of gas phase molecules. X-ray diffraction [3] can measure crystalline structures. Laser pump-probe techniques have high time resolution [4] but they cannot measure structure because of the long wavelength of optical photons. If the long wavelength photons could be converted into short wavelength particles (electrons or ions), then high spatial resolution could be combined with ultrafast temporal resolution. We use laser Coulomb explosion [5–7] for the conversion, producing short wavelength ions ($\lambda < 0.001$ nm).

A Coulomb explosion triggered by a high-velocity collision between a multi-MeV molecular ion and a thin foil was originally developed for measuring static molecular structures [8]. Rapid ionization also occurs during collisions between highly charged atoms and molecules [9], or during Auger decay following the absorption of x rays [10]. These studies advanced the technology of coincidence imaging. By using few-cycle pulses and coincidence imaging, we achieve sub-5 fs and sub-Å resolution of vibration and dissociation dynamics.

We initiate dynamics in D_2 and SO_2 by multiphoton ionization from a few-cycle pump pulse to D_2^+, SO_2^{2+}, and SO_2^{3+}. We image the time-dependent nuclear motion by laser Coulomb explosion imaging (CEI). We choose D_2^+ because of its extremely fast molecular motion [11]. We choose SO_2^{n+} for three reasons. First, we demonstrate that even when multiple dissociation channels simultaneously occur, CEI allows each to be imaged. Second, we image unstable radical ions produced by rapid ionization, which are otherwise very difficult to measure. Finally, SO_2^{2+} has a specific dissociation channel, $SO_2^{2+} \rightarrow O^+ + S^+ + O$ that is observed when x ray absorption induces rapid double ionization. Neither theory nor experiment has been able to determine if this channel is concerted or sequential [12]. We show that both bonds break simultaneously (concerted) when produced by rapid multiphoton ionization.

We generate the ~8 fs laser pulses by self-phase modulation of ~40 fs Ti:sapphire in an argon-filled hollow-core fiber and compression with chirped mirrors [5]. The pulse sits upon a ~5% intensity background lasting ~100 fs. To generate pump and probe with variable time delay, we use two pieces of 3-mm-thick fused silica: a 25-mm-diam annulus, and a 5-mm-diam disk which was the center of the annulus. The beam passing through the inner disk is the pump, and the outer beam is the probe. Rotating the annulus delays the probe with respect to the pump.

Our interaction chamber contains a uniform acceleration time-of-flight mass spectrometer (240 mm ion flight length, 70 mm internal diameter), and a position-sensitive detector that can measure the velocities of up to eight fragment ions per shot [5,13,14]. The detector efficiency is ~50%. For the D_2 experiments, the acceleration field is 100 V/cm and 250 V/cm for SO_2. The molecules enter the interaction chamber in a low-density beam that is ~50 μm thick along the laser beam propagation direction. There is less then one molecule per laser shot in the focus. We now describe how laser CEI can be used to observe vibrational dynamics in D_2^+.

As illustrated in Fig. 1(a), ionization of D_2 launches a vibrational wave packet in D_2^+. The pump intensity was $I_{\text{pump}} \sim 3 \times 10^{14}$ W/cm^2 and the probe intensity was $I_{\text{probe}} \sim 1 \times 10^{15}$ W/cm^2. At $I_{\text{pump}} \sim 3 \times 10^{14}$ W/cm^2, only single ionization to $D_2^+ X\,^2\Sigma_g^+$ is possible, resulting in a well defined D_2^+ wave packet. In addition, a significant fraction of molecules is ionized at this intensity. We only analyze data for molecules that are within 10° of being perpendicular to the laser polarization.

Figure 1(b) shows the kinetic energy spectrum of the D^+ fragments. Zero and 12 fs correspond to times of the smallest and largest expected bond length. The fragments in Fig. 1(b) have lower kinetic energy when the wave packet is probed at 12 fs than when it is probed at 0 fs. The high-energy tail in the experimental 12 fs spectrum is due to molecules that were not ionized by the pump pulse.

Figure 1(c) shows the fraction of fragments with energy

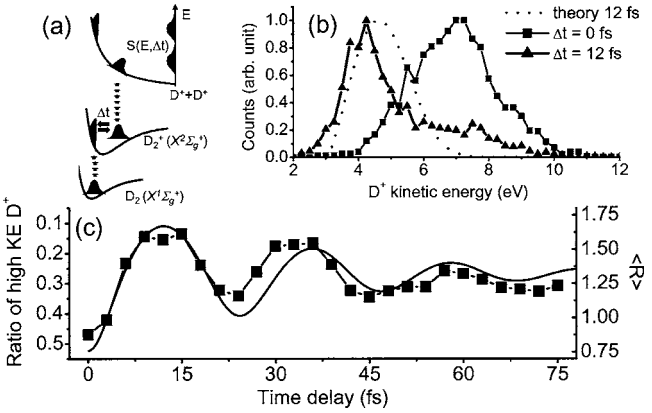

FIG. 1. (a) Potential energy surface of D_2^{n+} sketching the concept of the experiments. (b) D^+ kinetic energy (KE) spectra for a pump-probe delay of 0 fs (square) and 12 fs (triangle). The dotted curve is the expected kinetic energy spectrum for $\Delta t=12$ fs. (c) Ratio of high KE D^+ is the total number of D^+ counts having KE>7 eV divided by total D^+ counts (square). Calculated time-dependent average internuclear distance ($\langle R\rangle$ in Å) as a function of time on $D_2^+ X\,^2\Sigma_g^+$ (solid line). $I_{\text{pump}}\sim 3\times 10^{14}$ W/cm^2, $I_{\text{probe}}\sim 1\times 10^{15}$ W/cm^2.

greater than 7 eV over total D^+ counts (squares, left axis) as a function of the delay. We choose 7 eV because the $\Delta t=0$ fs spectrum peaks at this value. We follow the wave packet motion for 75 fs until it has mostly dephased. At longer time delays, beyond the reach of our 3-mm-thick disk/ (annulus) delay stage, we expect the wave packet to revive. A clear oscillation of fragment kinetic energy is visible, tracing the ultrafast dynamics of D_2^+.

For fragments parallel to the laser polarization, the agreement is only relatively good for delays less than 12 fs. At longer times, the strong parallel coupling between the $A\,^2\Sigma_u^+$ and $X\,^2\Sigma_g^+$ induced by the 5% background intensity of the probe pulse affects the wave packet motion. By choosing angles between 80° and 100° to laser polarization, this background has almost no effect on the wave packet motion.

We compare our experimental results with a simulation. We project the ground state wave function of D_2 onto the $D_2^+ X\,^2\Sigma_g^+$ surface, solve the time-dependent Schrödinger equation, and then project the wave packet onto the Coulomb potential. In Fig. 1(b), the dotted curve is the predicted spectrum at 12 fs. The solid line in Fig. 1(c) shows the average internuclear distance ($\langle R\rangle$, right axis) as a function of time on the $X\,^2\Sigma_g^+$ surface. The ~24 fs vibration period and ~60 fs dephasing time in Fig. 1(c) are consistent with our knowledge of the $D_2^+ X\,^2\Sigma_g^+$ state.

We now turn our attention to SO_2. A pump pulse, $I_{\text{pump}}\sim 1\times 10^{15}$ W/cm^2, removes up to three electrons from the SO_2 producing doubly and triply charged molecules. This launches a set of dissociative wave packets on both charge states. Since they dissociate, we can record the velocity vectors of all fragment ions produced by the pump alone. We identify five photodissociation channels: ($SO_2^{3+}\rightarrow O^+ + S^+ + O^+$); ($SO_2^{3+}\rightarrow SO^{2+}+O^+$); ($SO_2^{2+}\rightarrow SO^+ + O^+$); ($SO_2^{2+}\rightarrow O^+ + S^+ + O$), and ($SO_2^{2+}\rightarrow S^+ + O_2^+$). The three most probable channels are italicized.

A probe pulse, $I_{\text{probe}}\sim 5\times 10^{15}$ W/cm^2, explodes the dissociating molecules that were prepared by the pump. We observe charge states up to SO_2^{10+}. We only analyze events where all three fragments from the molecule (S^{i+}, O^{j+}, and O^{k+}) are captured. To guard against false coincidences, we require that the momentum sum of the three detected ions is less than 1×10^{-22} kg m/s. Fewer then 5% of the events are false coincidences.

A major question in the photochemistry of three-body dissociation is whether the process is concerted or sequential. Do the two bonds of SO_2^{n+} ($n=2$; $SO_2^{2+}\rightarrow O^+ + S^+ + O$; $n=3$: $SO_2^{2+}\rightarrow O^+ + S^+ + O^+$) break simultaneously? We can resolve this question for SO_2^{n+} with information from the explosion channel $SO_2^{7+}\rightarrow O^{2+}+S^{3+}+O^{2+}$. If both O^{2+} fragments have similar energy, we can conclude that the channel probed by the CEI is a concerted three-body breakup, if not, the dissociation is sequential.

Figure 2(a) presents the correlation map of the O^{2+}-O^{2+} kinetic energy. The 0 fs image was obtained by the CEI of SO_2 at its equilibrium position. At $\Delta t=220$ fs, the correlation map has broken into three distinct peaks; the low energy part that lies along the diagonal ($E_1=E_2\sim 9$ eV), and two off diagonal peaks ($E_1\sim 7$ eV, $E_2\sim 36$ eV). The labeling of O^{2+} as 1 or 2 is determined by which ion strikes the detector first. A background due to the CEI of nonexcited SO_2 has been subtracted from all maps (except 0 fs).

Figure 2(a) shows dynamics along the diagonal towards the lower energy as a function of time delay. Dynamics into diagonal indicates concerted three-body break up. An off diagonal dynamics appears 30 fs after ionization and becomes well separated at longer times. For the off-diagonal peaks of Fig. 2(a), the oxygen with high energy was still bonded to the sulfur, while the low energy oxygen came from the dissociating bond. At long delays, (e.g., $\Delta t=220$ fs) the dissociating oxygen is far from the sulfur, and receives negligible energy from the CEI. When we compare the O^{2+} energy after the CEI at $\Delta t=220$ fs with the energy of the O^+ coming from the dissociation of $SO_2^{2+}\rightarrow SO^+ + O^+$ when only the pump laser is on, we confirm that the asymmetric features in Fig. 2(a) are from SO_2^{2+} ions as they dissociate to $SO^+ + O^+$. We distinguish with femtosecond resolution concerted three-body break up from asymmetric dissociation.

There are actually two concerted channels, seen in Fig. 2(b). The channels show up as two isolated peaks when the angle between the velocity vectors of the O^{2+} fragments (α) is plotted as a function of the total energy for the events on the diagonal of Fig. 2(a) at $\Delta t=220$ fs. For the same reason as mentioned above, by choosing a long delay of 220 fs, we can compare the CEI data to the measurements with only the pump pulse. The narrower distribution, with an average energy of ~27.5 eV, has an α distribution corresponding to $SO_2^{3+}\rightarrow O^+ + S^+ + O^+$. The broader distribution, with an average energy of ~22.5 eV, has an α distribution corresponding to $SO_2^{2+}\rightarrow O^+ + S^+ + O$ (we determine the momentum of the unobserved O fragment by momentum conservation with the measured O^+ and S^+ from data where only the pump pulse interacts with SO_2). Thus, we confirm that $SO_2^{3+}\rightarrow O^+ + S^+ + O^+$ is concerted [12] and find that $SO_2^{2+}\rightarrow O^+ + S^+ + O$ breakup is also concerted.

The CEI is an imaging technique. So far, we have used

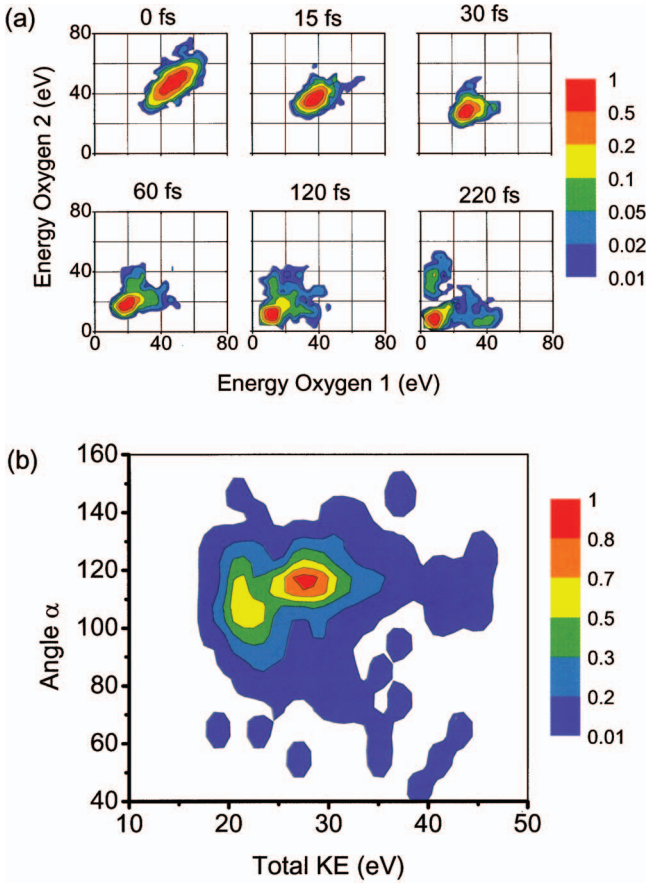

FIG. 2. (Color) (a) O^{2+} energy-energy correlation map. The final charge state is $SO_2{}^{7+} \rightarrow O^{2+}+S^{3+}+O^{2+}$ (the map is on a logarithmic scale). (b) Velocity angle vs total kinetic energy (eV) for pump-probe delay of 220 fs (the map is on a linear scale). $I_{\text{pump}} \sim 1\times10^{15}$ W/cm^2, $I_{\text{probe}} \sim 5\times10^{15}$ W/cm^2.

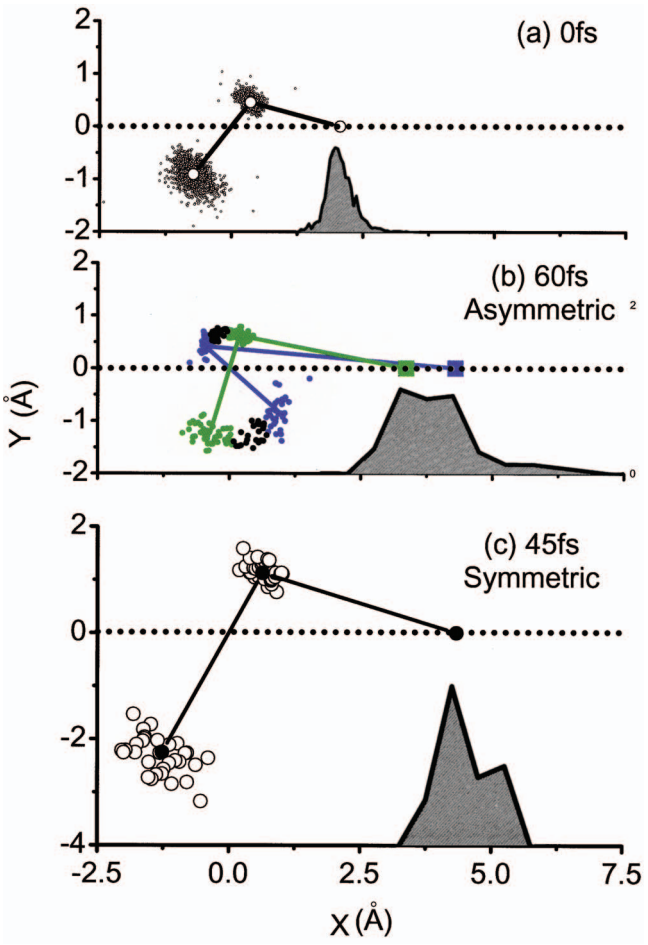

FIG. 3. (Color) (a) Structure of SO_2 at $\Delta t=0$ fs (final charge state is $SO_2{}^{7+} \rightarrow O^{2+}+S^{3+}+O^{2+}$). (b) Structure of $SO_2{}^{2+}$ undergoing asymmetric dissociation ($SO_2{}^{2+} \rightarrow SO^{+}+O^{+}$) at $\Delta t=60$ fs. Blue: average structure for bond angle $<50°$. Green: average structure for bond angle $>75°$ (final charge is $SO_2{}^{7+} \rightarrow O^{2+}+S^{3+}+O^{2+}$). (c) Structure of SO_2 in the concerted dissociation channel at $\Delta t=45$ fs, also shown is the equilibrium structure of SO_2 (final charge is $SO_2{}^{10+} \rightarrow O^{3+}+S^{4+}+O^{3+}$). $I_{\text{pump}} \sim 1\times10^{15}$ W/cm^2, $I_{\text{probe}} \sim 5\times10^{15}$ W/cm^2.

partial information to identify and qualitatively describe dissociation channels. Figure 3 shows three images determined from the measured velocity vectors. Although randomly aligned in space, each SO_2 ion explodes in a plane. Therefore, we can view all images in a single plane. We define the plane as follow: in all images, the center of mass of one SO^{n+} bond is set at (0,0). For asymmetric channels, we select the center of mass of the shorter bond. For concerted channels, we choose SO^{n+} randomly. For all images, the remaining oxygen ion position is set to $Y=0$ and X positive. This defines the X axis. We define the Y axis by requiring that the sulfur ion have a component in the positive Y direction. With the plane defined, we turn to the data in Fig. 3. On the X axis of Fig. 3 we plot the distribution of position of the $Y=0$ oxygen ion. To show some aspects of the correlation, the distribution in Fig. 3(b) is broken into three segments (green, black, and blue) and the average of the two outer distributions are shown as points. The lines connect the average positions.

The algorithm that we use to calculate structures assumes initial positions for each atom and uses classical motion on a Coulomb potential with zero initial velocities [14]. An iterative procedure converges on a structure that results in explosion velocities consistent with experimental results. For long delays, our zero initial velocity assumption is not accurate, so the images in Fig. 3 are only for delays of 60 fs or less.

To minimize the effect of nonzero initial velocities, we use the highest charge state available, $SO_2{}^{10+}$ for $SO_2{}^{3+} \rightarrow S^{+}+O^{+}+O^{+}$ and $SO_2{}^{2+} \rightarrow S^{+}+O^{+}+O$. We estimate a spatial resolution of $\leqslant 1$ Å and bond angle resolution of 15° for delays $\leqslant 45$ fs. For the asymmetric channel, $SO_2{}^{2+} \rightarrow SO^{+}+O^{+}$, there are insufficient $SO_2{}^{10+}$ explosions, so we use $SO_2{}^{7+}$. Similar spatial resolution is obtained for delays $\leqslant 60$ fs since the wave packet motion on the doubly charged state is slower.

The upper plot of Fig. 3 shows the measured SO_2 equilibrium structure ($\Delta t=0$ fs) probed by a $SO_2{}^{7+}$ explosion. The middle plot, taken at 60 fs, shows the asymmetric $SO_2{}^{2+} \rightarrow SO^{+}+O^{+}$ channel, also probed with $SO_2{}^{7+}$. The bottom, taken at 45 fs, shows the image of three-body breakup channels probed by $SO_2{}^{10+}$ explosions.

The $\Delta t=0$ fs image [Fig. 3(a)] has $R_1=R_2 \sim 1.7$ Å and an

average O-S-O angle of 120°, close to the known 119° equilibrium angle and 1.43 Å bond distance [15]. By $\Delta t=60$ fs [Fig. 3(b)], the average angle has decreased to ~70°, the unbroken bond distance has increased to 2 Å, and the atomic fragment has an average distance of ~3.7 Å from the center of mass of SO^+. Figure 3(b) shows that the angle is smaller for more rapidly moving O^+ fragments (longer distance from SO^+ center of mass). Thus, we observe the rotational wave packet created when the angular momentum is transferred during asymmetric dissociation. Figure 3(c) shows the three-body breakup channels at $\Delta t=45$ fs. At 45 fs, we cannot distinguish between the $SO_2^{2+}\rightarrow S+O^+ +O^+$ and the $SO_2^{3+}\rightarrow S^+ +O^+ +O^+$ channels. We measure $R_1=R_2\sim 4.1$ Å and the average bond angle has decreased from 120° to 100°.

Before concluding, it is important to discuss the accuracy of our measurements. The images in Fig. 3 come from the measured ion velocities. The main error comes from the pixelization of the detector (250 μm). This corresponds to an uncertainty in the velocity of ~250 m/s. In our experiments, a typical final velocity is on the order of 10 000 m/s. We estimate that such an experimental error can cause a bond angle error of 5° and a bond distance error of ~0.1 Å in Fig. 3.

In conclusion, our results show that current laser technology allows the dynamics of small molecules to be imaged in time steps of 5 fs. The CEI allows a full image to be taken from each explosion. This single molecule imaging capability lets us follow a complex photochemical process—the asymmetric dissociation of SO_2^{2+}—and distinguish it from concerted dissociation.

Looking ahead laser CEI will allow photochemical processes in small neutral molecules to be imaged frame by frame. Image quality will improve because of the lower energy of neutral molecule dissociation and from using shorter, 3.4 fs explosion pulses [16]. 0.1 Å resolution images [5,14] with ~2 fs between consecutive frames seems possible. In addition, laser CEI will allow statistical breakup to be imaged, a process that is very important in chemistry. One important issue in statistical breakup is the structure(s) that the molecule assumes it dissociates. By imaging one molecule at a time, laser CEI can distinguish molecules that are fragmenting during predissociation from the much more common but less interesting molecules that are already fragmented or are yet to fragment.

We thank Professor K. Yamanouchi (University of Tokyo) for stimulating discussions. The authors appreciate financial support from the NSERC, the NRC/CNRS collaborative research fund, the CIPI, and the FQRNT.

[1] A. H. Zewail, J. Phys. Chem. A **104**, 5660 (2000).
[2] H. Ihee, V. A. Lobastov, U. M. Gomez, B. M. Goodson, R. Srinivasan, C.-Yu Ruan, and A. H. Zewail, Science **291**, 458 (2001).
[3] F. Schotte, M. Lim, T. A. Jackson, A. V. Smirnov, J. Soman, J. S. Olson, G. N. Phillips, Jr., M. Wulff, and P. A. Anfinrud, Science **300**, 1944 (2003).
[4] T. Saito and T. Kobayashi, J. Phys. Chem. A **106**, 9436 (2002).
[5] F. Légaré, I. V. Litvinyuk, P. W. Dooley, F. Quéré, A. D. Bandrauk, D. M. Villeneuve, and P. B. Corkum, Phys. Rev. Lett. **91**, 093002 (2003).
[6] K. Zhao, G. Zhang, and W. T. Hill, III, Phys. Rev. A **68**, 063408 (2004).
[7] C. Beylerian and C. Cornaggia, J. Phys. B **37**, L259 (2004).
[8] E. P. Kanter, P. J. Cooney, D. S. Gemmell, K.-O. Groeneveld, W. J. Pietsch, A. J. Ratkowski, Z. Vager, and B. J. Zabransky, Phys. Rev. A **20**, 834 (1979).
[9] D. Mathur, Phys. Rep. **391**, 1 (2004).
[10] A. De Fanis, N. Saito, M. Machida, K. Okada, H. Chiba, A. Cassimi, R. Dörner, I. Koyano, and K. Ueda, Phys. Rev. A **69**, 022506 (2004).
[11] B. Feuerstein and U. Thumm, Phys. Rev. A **67**, 063404 (2003).
[12] S. Hsieh and J. H. D. Eland, J. Phys. B **30**, 4515 (1997).
[13] P. W. Dooley, I. V. Litvinyuk, Kevin F. Lee, D. M. Rayner, D. M. Villeneuve, and P. B. Corkum, Phys. Rev. A **68**, 023406 (2003).
[14] F. Légaré *et al.*, Phys. Rev. A **71**, 013415 (2005).
[15] *CRC Handbook of Chemistry and Physics* (CRC Press, Boca Raton, 2003).
[16] K. Yamane, Z. Zhang, K. Oka, R. Morita, M. Yamashita, and A. Suguro, Opt. Lett. **28**, 2258 (2003).